Molecular dynamics simulations of nanometric metallic multilayers: Reactivity of the Ni-Al system

Florence Baras, Olivier Politano

▶ **To cite this version:**

Florence Baras, Olivier Politano. Molecular dynamics simulations of nanometric metallic multilayers: Reactivity of the Ni-Al system. Physical Review B: Condensed Matter and Materials Physics (1998-2015), 2011, 84, pp.024113. 10.1103/PhysRevB.84.024113 . hal-00645520

HAL Id: hal-00645520
https://hal.science/hal-00645520

Submitted on 28 Nov 2011

HAL is a multi-disciplinary open access archive for the deposit and dissemination of scientific research documents, whether they are published or not. The documents may come from teaching and research institutions in France or abroad, or from public or private research centers.

L'archive ouverte pluridisciplinaire **HAL**, est destinée au dépôt et à la diffusion de documents scientifiques de niveau recherche, publiés ou non, émanant des établissements d'enseignement et de recherche français ou étrangers, des laboratoires publics ou privés.

Molecular dynamics simulations of nanometric metallic multilayers: Reactivity of the Ni-Al system

Florence Baras and Olivier Politano

Laboratoire Interdisciplinaire Carnot de Bourgogne, UMR 5209 CNRS-Université de Bourgogne, 9 Avenue A. Savary, Boîte Postale 47 870, F-21078 Dijon Cedex, France

(Received 17 May 2011; published 12 July 2011)

The reactivity of a layered Ni-Al-Ni system is studied by means of molecular dynamics simulations, using an embedded-atom method type potential. The system, made of an fcc-Al layer embedded in fcc-Ni, is initially thermalized at the fixed temperature of 600 K. The early interdiffusion of Ni and Al at interfaces is followed by the massive diffusion of Ni in the Al layer and by the spontaneous phase formation of $B2$-NiAl. The solid-state reaction is associated with a rapid system heating, which further enhances the diffusion processes. For longer times, the system may partly lose some its $B2$-NiAl microstructure in favor of the formation of $L1_2$-Ni_3Al. This stage is controlled by the diffusion of Al in the Ni-rich phase, and a layer-by-layer development of the new phase is observed.

DOI: 10.1103/PhysRevB.84.024113 PACS number(s): 64.70.Nd, 02.70.Ns, 68.35.bd

I. INTRODUCTION

Nanometric metallic multilayers (N2M's) are obtained by the superposition of very thin A-B films, where A and B are pure metals. The layer thickness typically varies between a few to 100 nanometers and the number of layers may be extremely large, about 5000. Such multilayer nanofilms are now easily produced by a magnetron sputtering technique or high-vacuum deposition (for a relatively small number of layers). Because of their interesting applications in many modern technologies,[1–3] the production of N2M's has increased considerably during the past decade. Concomitantly, their study attracts more and more attention (for a recent review, see Ref. 4).

The N2M is chemically stable if A and B are nonmiscible. Otherwise, A and B will first mix into a solid solution and then react to give intermetallics compounds. Since the material is made of alternating very thin layers, it may become highly reactive even at low temperature and the reaction proceeds quite rapidly. N2M's are thus well suited for welding and soldering heat-sensitive materials in a few seconds without damage. The performance and the efficiency of N2M are directly related to the promotion or the inhibition of reactions such as compound formation, crystallization, or grain growth.

To understand the behavior of such systems, it is thus necessary to study the dynamics of phase and structural transformations associated with heterogeneous reactions at nanoscale. Since this kind of nano-object is essentially made of interfaces, it raises many questions about the role of huge concentration gradients in the nucleation process, the limiting role of diffusion on the reaction, the presence of defects due to the misfit in the lattice parameters, and the real possibility of crystallization in nanosystems. Besides the very powerful experimental techniques that are now available to study N2M's, such as time-resolved x-ray diffraction (TRXRD) using synchrotron radiation or differential scanning calorimetry (DSC), it is interesting to develop an appropriate modeling of these nanosystems. Molecular dynamics (MD) seems to be a promising tool to study N2M's since the typical length scales (a few nanometers) correspond precisely to the ones accessible by the simulation. Moreover, a great effort has been made to develop interatomic potentials for binary metallic systems and their alloys.

Molecular dynamics has been used successfully to study the interface between crystalline copper and liquid aluminum,[5] the demixing phenomena in NiAl nanosized particles,[6] the melting and crystal growth in $Al_{50}Ni_{50}$ system,[7] the sintering process and the alloying between Al and Ni nanoparticles,[8] the exothermic alloying of Ni/Al multilayers induced by shock loading,[9,10] or to determine the pressure-dependent melting temperature of Al and Ni.[11] This method has also been used to investigate the interfacial mixing behavior in transition metal (Fe,Co,Ni)-Al multilayer systems during deposition[12] or to study the atomic scale structure of sputtered metal multilayers.[13]

II. DETAILS OF THE SIMULATION

In this work, we study a layered Ni-Al-Ni system by molecular dynamics using an embedded-atom method (EAM).[14] We use the specific potential developed by Mishin *et al.*[15] that has been constructed for the intermetallic compound $B2$-NiAl as well as for Ni and Al by fitting to both experimental properties and *ab initio* data. The potential accurately reproduces the basic lattice properties of $B2$-NiAl and the energetics and stability of other structures like $L1_2$-Ni_3Al. As compared to a real Ni-Al system, the potential deals with a simplified system with a limited number of phases. The MD simulation is conducted using the LAMMPS software package.[16]

We choose a simplified geometry (see Fig. 1) of a layered Ni-Al-Ni system to model alternating continuous very thin layers of Ni and Al. The system is made of one layer of Al (9 atomic planes form the inner layer) in between two Ni layers of 11 atomic planes each (the outer layers) along the z direction. Both pure metals are in fcc configuration and the interface orientation is (001). The width in the x and y directions of the Al layer is chosen to be smaller than the Ni layers [$L_x(\mathrm{Al}) < L_x(\mathrm{Ni})$ and $L_y(\mathrm{Al}) < L_y(\mathrm{Ni})$]. The typical size of the simulation box is $L_x = L_y \approx 10$ nm and $L_z = 5.6$ nm. The system is submitted to periodic boundaries conditions in all directions. The specific geometry with a narrower Al layer allows us to avoid artificial constraints due to the application of periodicity on both Al and Ni layers during the construction of the system. This way, the system around the interface is able to manage the misfit between the two

 ©2011 American Physical Society

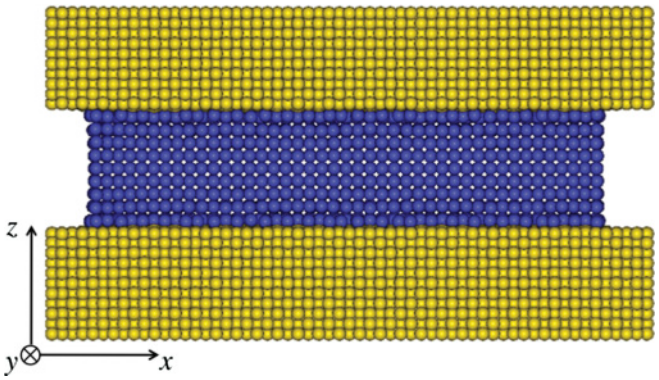

FIG. 1. (Color online) Initial configuration of the simulated system with one Al slice in between two Ni layers. Al and Ni are shown as blue (black) and yellow (white) spheres, respectively.

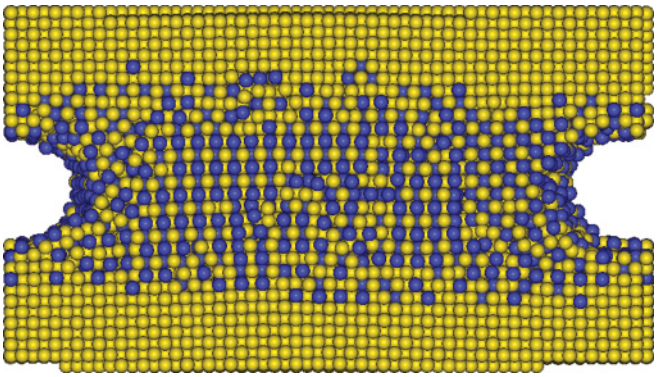

FIG. 2. (Color online) Snapshot of the simulated configuration with two Ni-Al interfaces, at $t = 6$ ns, sliced for $y > 10$ Å. Al and Ni are shown as blue (black) and yellow (white) spheres, respectively. We note that the middle Al layer is curved due to the wetting.

crystalline structures. It also appears that the initial distance δ between the Ni- and Al-atomic planes around the interface may considerably influence the later evolution. A detailed analysis will be presented in a forthcoming publication. In this work, we present the results obtained for a value of $\delta = 2.5$ Å, which corresponds to a system's potential energy close to its minimum at 0 K and allows us to preserve the fcc local structure of the majority of both Ni and Al atoms. In this case, the Al layer is in traction [the interlayer distance d_{ij} slightly exceeds the lattice parameter a_0(Al)] while the Ni layer is somewhat shrunk [$d_{ij} < a_0$(Ni)].

The system is made of 43 643 atoms [n(Al) = 8321 and n(Ni) = 35 322]. Both Al and Ni lattice parameters were determined at 600 K on bulk systems by using isothermal-isobaric (NPT) simulations (see Table I). Hence, the Ni-Al-Ni system is created at 600 K with the appropriate lattice parameters and thermalized using simulations in the canonical statistical ensemble (NVT) over 400 ps. The simulation is then carried out in the microcanonical statistical ensemble (NVE) over more than 20 ns. A snapshot of the system at $t = 6$ ns is shown in Fig. 2.

Several indicators allow us to follow the evolution of the system at the microscopic level. The number density profiles in the direction perpendicular to the interface give an indication of the crystallinity state and of the local composition n_i in Ni or Al in each slice i. Well-defined peaks are typically associated with a solid system structured in atomic planes. If we calculate the *local lattice structure* according to the formulation given by Ackland,[17] we get the local configuration around a given atom based not on the distance between particles but the angles. It is possible to distinguish between five configurations: bcc ($a = 1$), fcc ($a = 2$), hcp, ico, and unknown. So each atom is labeled by the color of the species and by its local lattice structure. To determine the phase to which a given atom belongs, its potential energy can be compared to the potential energy of the same species atom in the structure corresponding to the phase. As shown in Table I, the potential energy of Ni in pure Ni, in NiAl, or in Ni_3Al may be significantly different. To identify the lattice arrangement of a set of atoms (for instance, in an atomic plane), it is also possible to compute the histogram of pairwise distances (hpd) for all atoms in the set. This gives a quantity very similar to an unnormalized radial distribution function. This quantity can then be compared to the successive interatomic distances of a given structure, such as, for instance, $B2$-NiAl.

TABLE I. Lattice parameter a_0 (Å) and cohesive energy E_0 (eV) of the Ni-Al compounds at 600 K. The second column corresponds to the lattice structure. The notation E_{Ni} indicates the potential energy of an atom of Ni in a given structure. The last column is the atomic density ρ (at/nm^3) at 600 K.

Phase		a_0	E_0	E_{Al}	E_{Ni}	ρ
Ni	$A1$	3.482	−4.493		−4.493	94.75
Ni_3Al	$L1_2$	3.561	−4.593	−3.295	−5.025	88.58
NiAl	$B2$	2.886	−4.460	−3.551	−5.369	84.37
Al	$A1$	4.087	−3.359	−3.359		58.59

III. RESULTS

During the thermalization period at 600 K, the main transformations appear in the inner layer. To deal with the crystallographic misfit and with the traction, Al atoms wet the free surface of Ni at the interfaces. This leads to the formation of defects in the Al atomic planes as vacancies or line defects that break the perfect symmetry of the planes. Sectors of fcc Al atoms are separated by two-dimensional grain boundaries. Due to the spontaneous adjustment of Al atoms close to the interface, the interplane distance d_{ij} in the inner Al layer becomes very close to the lattice parameter of Al at 600 K.

During the NVE simulation, it is interesting to follow global quantities for the overall system. Figure 3 shows the evolution of the temperature together with the total number of atoms that are in a local configuration bcc and fcc. The temperature rise is accompanied with a structural modification of the system as fcc atoms are disappearing in favor of bcc atoms. In other words, while the total energy is conserved, there is an exchange between potential and kinetic energy in the system. It is particularly interesting to understand the spontaneous evolution of the system, in particular the development of an exothermic behavior, which reveals the extreme reactivity of the system. For this purpose, we analyze the different stages in the evolution.

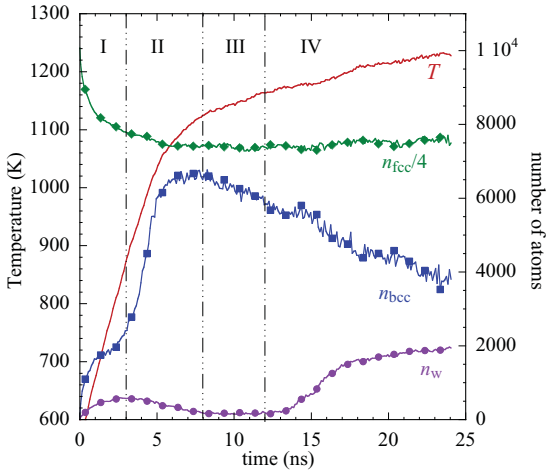

FIG. 3. (Color online) Temperature T (scale in K, on the left) and number of atoms (on the right) as a function of time (scale in ns). The number of atoms in local configuration bcc ($a = 1$) is indicated by squares, one-quarter of the number of atoms in local configuration fcc ($a = 2$) by diamonds, and the number of wetting atoms n_w by bullets. The different stages in the evolution are indicated by the dashed-dotted lines.

Just after the thermalization, from $t = 0.4$ to 3 ns (stage I), the Al slice becomes amorphous. There is no more clear evidence of atomic planes and Ni atoms start to invade the zone, as shown in Fig. 4(a). On the other hand, the Al atoms diffusing in the Ni slices occupy the empty places liberated by outgoing Ni atoms and the atomic planes are not altered by the presence of Al atoms. As soon as the quantity of Ni is sufficient, the middle slice recovers its crystallinity. During

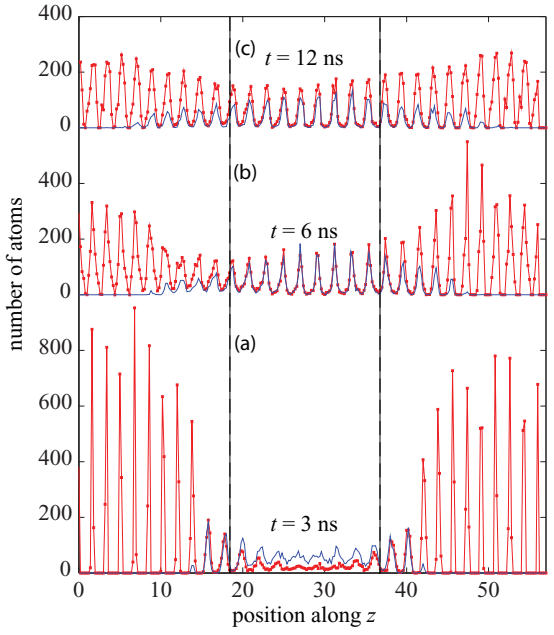

FIG. 4. (Color online) Number density profiles at $t = 3$, 6, and 12 ns in the direction z, perpendicular to the interfaces. The dashed lines indicate the limits of the inner Al layer in the initial configuration. The Ni profile is plotted with small bullets and the full line corresponds to the Al profile. Position is measured in angstroms.

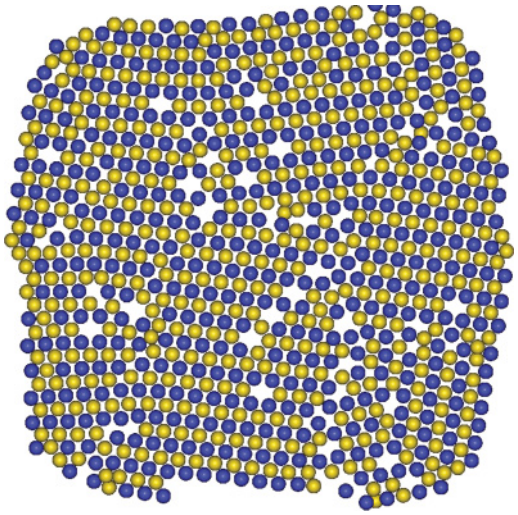

FIG. 5. (Color online) Snapshot of a slice (24 Å $< z <$ 26 Å) in the inner layer at $t = 6$ ns. Al and Ni are shown as blue (black) and yellow (white) spheres, respectively. The atomic arrangement is characteristic of a (110) orientation in NiAl.

stage II (from $t = 3$ to 8 ns), the number of bcc atoms abruptly increases together with temperature. The location of bcc atoms is in the inner layer. This behavior could be associated with an exothermic reaction between nickel and aluminum, giving rise to the formation of the compound NiAl,

$$\mathrm{Ni} + \mathrm{Al} \rightarrow \mathrm{NiAl}. \tag{1}$$

If we make the strong hypothesis that the Ni atom keeps its cohesive energy until the reaction takes place, the energy balance expressed in terms of cohesive energies reads (see Table I)

$$\tfrac{1}{2}\,[E_0(\mathrm{Ni}) + E_0(\mathrm{Al})] = E_0(\mathrm{NiAl}) + q, \tag{2}$$

where $q = 0.54$ eV is the excess of energy liberated by the atomic rearrangement. On the one hand, the number of Al and Ni atoms progressively reaches the 1:1 stoichiometry required to form the intermetallic [see Fig. 4(b)]. On the other hand, each atomic plane shows alternating lines of Ni and Al atoms in sectors of around 5–6 nm^2 (see Fig. 5). This qualitative aspect is corroborated more quantitatively by the histogram of pairwise distances in each plane. In Fig. 6(a), the pairwise distances measured between Ni-Ni, Al-Al, and Ni-Al bcc atoms are compared to the values expected for NiAl. We note an excellent agreement. It appears that the new atomic structure rests on a simple cubic lattice whose lattice parameter is very similar to the fcc lattice of Al. The distance d_{ij} between Al planes in the middle layer remains close to the lattice parameter $a_0(\mathrm{Al})/2$. The fcc Al is characterized by 4 atoms/cell while the bcc NiAl cell contains only one atom of Al. Therefore, if we consider a build up of NiAl based on the existing Al lattice, only one Al atom from fcc Al can stay in the new NiAl lattice. The maximum number of Al atoms in the middle layer that occupy bcc positions is thus limited to a quarter of the initial number (around 230 atoms in each plane). This is precisely what is observed in the simulation. Around half of the atoms (Ni or Al) have a local lattice structure $a \neq 1$ and occupy the borders of the layers or

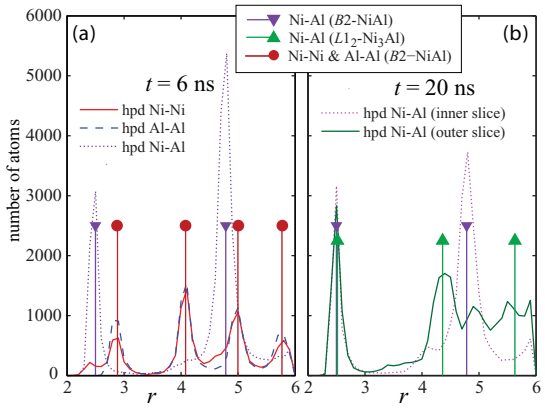

FIG. 6. (Color online) (a) Histograms of pairwise distances (hpd), at $t = 6$ ns, between Ni and Ni (solid line), Al and Al (dashed line), and Ni and Al atoms (dotted line). (b) hpd, at $t = 20$ ns, between Ni and Al atoms, in two representative slices of the inner (dotted line) and outer (solid line) layers. Vertical straight lines correspond to the theoretical values of the interatomic distances for $B2$-NiAl and $L1_2$-Ni_3Al. Distance is measured in angstroms.

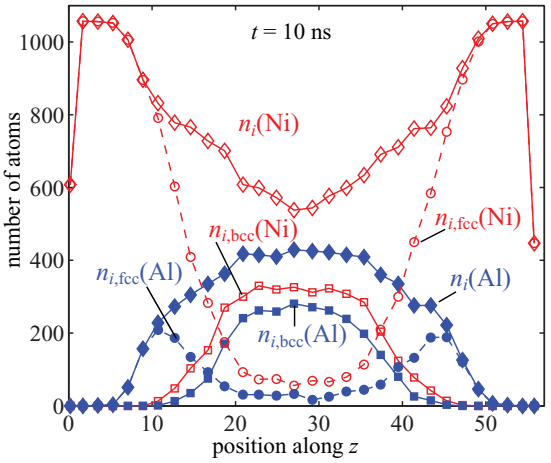

FIG. 7. (Color online) Local number of atoms n_i in a slice i along z at $t = 10$ ns. Ni species are represented by hollow markers and Al by full ones. The local number of atoms n_i is indicated by diamonds, the local number of bcc atoms $n_{i,\mathrm{bcc}}$ by squares, and the local number of fcc atoms $n_{i,\mathrm{fcc}}$ by bullets. Position is measured in angstroms.

the defect lines inside each slice. This corroborates the fact that only a local crystallization can spontaneously develop in the system. Around $t = 4$ ns, the formation of the new phase NiAl has already taken place in atomic planes near the interfaces. At $t = 6$ ns, all the planes show the crystallization phenomenon. As shown in Fig. 3, the system then reaches the maximum number of bcc atoms and stays on this plateau value for a while before a slow decrease in bcc atoms. The maximum temperature during stage II remains lower than 1100 K.

Stage III, which covers the period from $t = 8$ to 12 ns, can be considered a transient stage. The rise in temperature becomes less steep (10 K/ns) and the number of atoms in local bcc configuration decreases by 6% over this period. The measurement of the density along z shows well distinct peaks [see Fig. 4(c)] even if locally some atoms may join the adjacent atomic plane in the outer layers (larger peaks). The Al atoms that diffuse in Ni occupy substitutional positions in the fcc lattice of nickel. Anyway, Al atoms with $a = 2$ are observed close to the interfaces in the upper and lower layers. In these layers, the local stoichiometric ratio x_i [$x_i = n_i(\mathrm{Al})/n_i(\mathrm{Ni})$] is close to 0.33. A typical situation is illustrated in Fig. 7. One wonders if the solid solution will evolve and give rise to the formation of another phase. During the diffusion of Al atoms in the Ni substrate, Al atoms start to occupy vacancies liberated by diffusing Ni atoms. As soon as the number of Al atoms is locally sufficient (1 at/cell), a local reorganization takes place with the formation of the Ni_3Al compound. The balance energy for the cohesive energy per atom reads

$$\tfrac{1}{4}\,[3 \times E_0(\mathrm{Ni}) + E_0(\mathrm{Al})] = E_0(\mathrm{Ni_3Al}) + q' \qquad (3)$$

with $q' = 0.38$ eV the excess of energy liberated by the atomic rearrangement. Note that the exothermicity of this reaction is less than that for Eq. (1). This can partly explain the slower heating observed during stage III. Figure 8 shows the histogram of potential energy per atom for all atoms outside the inner layer. At the end of stage III ($t = 12$ ns), the distribution becomes bimodal. The peak associated with pure Ni drops and a second peak appears around the value E_{Ni} in Ni_3Al. This demonstrates the formation of a new phase Ni_3Al in the outer layers induced by the diffusion of Al in Ni substrate.

Due to the specific geometry of our model, the system is subjected to a wetting phenomenon. During stage I, Al atoms wet the free surfaces of nickel. The inner layer of aluminum slips and spreads on the nonrepellent free Ni surfaces at the borders of the system. This allows the Al layer to freely adjust the misfit of the lattice parameter. The wetting induces the defects, observed from the first moments of the simulation, which will play an essential role in the progress of diffusion and, actually, of reaction. By the way, the outer Ni layers, submitted to periodic boundary conditions, may be considered as a rigid substrate. The importance of wetting is measured by the number of atoms n_w outside a central parallelepiped

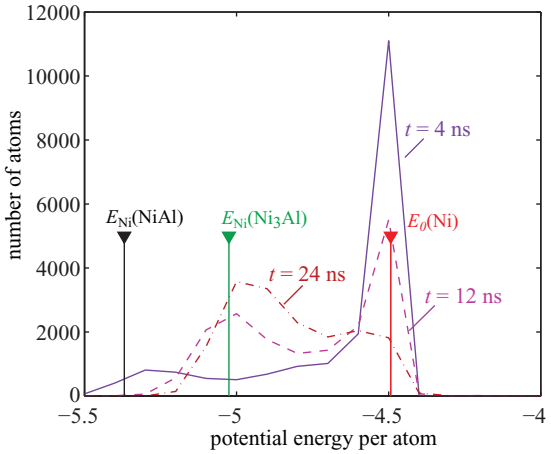

FIG. 8. (Color online) Histogram of potential energies per atom for all the Ni atoms in the outer layers. Full line, dashed line, and dashed-dotted line correspond to $t = 4$, 12, and 24 ns, respectively. Vertical straight lines indicate the theoretical values of the potential energy per atom in a given phase. Energy is measured in eV.

([0,90],[0,90],[18.6,37.6]) (see Fig. 3). As soon as Ni starts to diffuse in the Al layer, Ni atoms are also found in the wetting zone. During stage II, n_w is decreasing. This is due to the formation of NiAl, whose density is larger than pure Al. The wetting phenomenon is stable during stage III. Contrariwise, n_w sharply increases after $t = 12$ ns. Most of them are Ni atoms. We will see that this evolution stage corresponds to the formation of Ni_3Al in the outer layers. Since the density of Ni_3Al is much lower than the density of pure Ni (see Table I), the ejected Ni atoms will occupy the free space left around the inner layer.

The long-time behavior is associated with stage IV, from $t = 12$ to 24 ns. A slow heating is still observed (5 K/ns) while the number of atoms in a local bcc configuration is decreasing and the number of atoms in an fcc local environment is relatively stable. The careful study of the atomic planes gives a good insight into the system's evolution. Well-defined density peaks demonstrate the persistence of a solid-state evolution. Even if the system is heated during the progress of the reaction, the temperature stays lower that the melting temperature of Ni, NiAl, and Ni_3Al even at such nanoscales. Aluminum is supposed to melt around 1000 K for nanosystems. Note that, in the nanolayered system considered, Al has already reacted with Ni before the temperature has reached this value. This prevents the system from melting. In the inner layer, bcc atoms progressively disappear close to the interface while bcc atoms are still present in the core. In the outer layers, most of the Al atoms that have migrated have an fcc local configuration. They are first located near the interfaces, then increasingly far. Moreover, for these slices, the stoichiometric ratio x_i is close to the one expected for Ni_3Al. The histogram of the potential energies per atom computed for Ni atoms outside the central box shows that the peak centered around $E_{Ni}(Ni_3Al)$ becomes dominant. Moreover the hpd, calculated in a representative slice in the outer layer, reveals that the Ni-Al interdistance is located around the one expected for Ni_3Al [see Fig. 6(b)]. Contrariwise, the same analysis inside the inner layer shows the persistence of NiAl. It is interesting to follow how Al atoms will invade the overall system. The thickness of the layer containing Al atoms increases by successive jumps. This shows the progressive diffusion of Al in the Ni substrate and, by the way, the possibility of phase transformation in Ni_3Al.

IV. CONCLUSION

In this system, the crystallization of NiAl is spontaneous since it develops even in the absence of any nucleus. The NiAl compound first appears at the Ni-Al interface. But the existence of line defects in atomic planes promotes the rapid diffusion of Ni, which is further enhanced by the rise in temperature associated with the formation of NiAl. The NiAl phase formed in the core of the inner layer self-organizes in the small area (6 nm^2) delimitated by the line defects. Atoms of aluminum leaving the inner layer react with the nickel of the outer layers to form a new phase rich in nickel, Ni_3Al, near the interfaces. The new layer develops in the direction perpendicular to the interface. The phase growth is limited by the diffusion of Al thorough the new phase and takes place layer by layer. Concomitantly, Ni atoms diffuse in this opposite direction. The excess of Ni in the substrate acts as a reservoir, which maintains the system out of equilibrium. As a consequence, the diffusion flux of Ni in the inner layer partly destabilizes the NiAl formed at the very beginning of the reaction.

Our study enables us to detect the mechanisms responsible for the reaction in thin films at nanoscales and to analyze the microstructure obtained after the reaction. This approach could be valuably extended to understand the influence of the films' thickness, stoichiometry between metals, or initial temperature.

ACKNOWLEDGMENTS

The authors would like to thank S. Garruchet and A. L. Garcia for helpful discussions. The use of computational facilities at the Computing Center of the University of Bourgogne, DSI-CCUB, is gratefully acknowledged.

[1] T. P. Weihs, in *Handbook of Thin Film Process Technology*, edited by D. A. Glocker and S. I. Shah (IOP, Bristol, 1998).
[2] J. Wang, E. Besnoin, A. Duckham, S. J. Spey, M. E. Reiss, O. M. Knio, and T. P. Weihs, J. Appl. Phys. **95**, 248 (2004).
[3] A. J. Swiston Jr., E. Besnoin, A. Duckham, O. M. Knio, T. P. Weihs, and T. C. Hufnagel, Acta Mater. **53**, 3713 (2005).
[4] A. S. Rogachev, Russ. Chem. Rev. **77**, 21 (2008).
[5] P. Geysermans, D. Gorse, and V. Pontikis, J. Chem. Phys. **113**, 6382 (2000).
[6] F. Delogu, Nanotechnology **18**, 065708 (2007).
[7] A. Kerrache, J. Horbach, and K. Binder, Europhys. Lett. **81**, 58001 (2008).
[8] B. J. Henz, T. Hawa, and M. Zachariah, J. Appl. Phys. **105**, 124310 (2009).
[9] S. Zhao, T. C. Germann, and A. Strachan, J. Chem. Phys. **125**, 164707 (2006).
[10] S. Zhao, T. C. Germann, and A. Strachan, Phys. Rev. B **76**, 104105 (2007).
[11] N. S. Weingarten, W. D. Mattson, and B. M. Rice, J. Appl. Phys. **106**, 063524 (2009).
[12] S.-G. Lee and Y.-C. Chung, J. Appl. Phys. **105**, 034902 (2009).
[13] X. W. Zhou, H. N. G. Wadley, R. A. Johnson, D. J. Larson, N. Tabat, A. Cerezo, A. K. Petford-Long, G. D. W. Smith, P. H. Clifton, R. L. Martens, and T. F. Kelly, Acta Mater. **49**, 4005 (2001).
[14] R. A. Johnson, Phys. Rev. B **39**, 12554 (1989).
[15] Y. Mishin, M. J. Mehl, and D. A. Papaconstantopoulos, Phys. Rev. B **65**, 224114 (2002).
[16] See [http://lammps.sandia.gov/]; S. Plimpton, J. Comput. Phys. **117**, 1 (1995).
[17] G. J. Ackland and A. P. Jones, Phys. Rev. B **73**, 054104 (2006).